Environmental Science
Processes & Impacts

Determining Wavelength-Dependent Quantum Yields of Photodegradation: Importance of Experimental Setup and Reference Values for Actinometers

Journal:	*Environmental Science: Processes & Impacts*
Manuscript ID	EM-ART-02-2024-000084.R1
Article Type:	Paper

SCHOLARONE™
Manuscripts

Determining Wavelength-Dependent Quantum Yields of Photodegradation: Importance of Experimental Setup and Reference Values for Actinometers

Luana de Brito Anton[1], Andrea I. Silverman[1], and Jennifer N. Apell[1*]

[1]Civil and Urban Engineering Department, Tandon School of Engineering, New York University, Brooklyn, New York 11201, United States

*Corresponding author: japell@nyu.edu

ABSTRACT

Accurate quantum yields are crucial for modeling photochemical reactions in natural and engineered treatment systems. Quantum yields are usually determined using a single representative light source such as xenon lamps to mimic sunlight or UVC light for water treatment. However, photodegradation modeling can be improved by understanding the wavelength-dependence of quantum yields and the potential errors introduced by the experimental setup. In this study, we investigated the effects of experimental setup on measured quantum yields using four photoreactor systems and up to 11 different light sources. When using a calibrated spectroradiometer to measure incident irradiance on an open solution surface, apparent quantum yields were up to two times higher if light reflection and light screening were not accounted for in the experimental setup. When the experimental setup was optimized to allow for accurate irradiance measurements, quantum yields were reproducible across photoreactors. The optimized experimental setup was then used to determine quantum yields of the optically transparent solutions of uridine, atrazine, p-nitroanisole (PNA), sulfamethoxazole, and diclofenac across the UV spectrum. No significant wavelength dependence of quantum yields was observed for sulfamethoxazole and diclofenac, in

contrast to wavelength-dependent quantum yields for uridine, atrazine, and PNA. These reference values can be used for determining wavelength-dependent quantum yields of other compounds of interest. Additionally, more accurate results can be obtained when (1) it is possible to choose an actinometer with similar light absorption and photoreactivity compared to the target chemical, (2) when using optically transparent actinometers that can account for light reflection within reaction vessels, and (3) when using a quantum yield that corresponds to the spectra of the selected light source.

ENVIRONMENTAL SIGNIFICANCE

Quantum yields are necessary for modeling direct photolysis of chemicals in the natural environment and engineered treatment systems. This work quantifies the impacts of the experimental setup in calculating quantum yields and provides quantum yields across the UV spectrum for uridine, atrazine, p-nitroanisole (PNA), sulfamethoxazole, and diclofenac. These quantum yields can be used as reference values to more accurately characterize and model the photodegradation of chemicals of interest.

INTRODUCTION

Photochemical reactions can be important pathways for the degradation of anthropogenic chemicals and the biogeochemical cycling of naturally occurring compounds such as dissolved organic matter.(1, 2) These reactions occur in both the natural environment and engineered UV treatment systems.(3-6) To quantify the rates of these reactions, and thus understand their relative importance, quantum yields (Φ) of photolysis are typically measured in the laboratory and used to model photodegradation in a variety of systems.(7-10) Model accuracy is limited by the

uncertainty in the inputs, and uncertainties in Φ values are commonly driven by incorrect characterization of the spectral irradiance emitted by the light source used during experiments. When a calibrated spectroradiometer is not available or the experimental setup precludes its use (e.g., with bulbs on multiple sides of a merry-go-round photoreactor), the spectral irradiance is commonly measured using actinometry by quantifying the transformation of an actinometer. An actinometer is a photosensitive chemical with a well-characterized molar absorptivity and photolysis Φ that should not produce photoproducts that interfere with the absorbance of the actinometer itself.(11-14) Actinometers are often favored over spectroradiometers for measuring photon irradiances in photochemical experiments because they do not require regular calibration, can capture light reflections and fluctuations in intensity when irradiated alongside target solutions, and are adaptable to diverse experimental setups with varying geometries. Therefore, knowing the Φ of actinometers is critical for determining the Φ of other chemicals of interest and thus predict their photodegradation in the natural environment and engineered treatment systems.

A growing number of studies have focused on quantifying wavelength-dependent quantum yields (Φ_λ) to increase the accuracy and ability to model photodegradation rates in different environmental and treatment systems as well as to study photodegradation mechanisms.(15-20) This pursuit has been aided by the increased availability of monochromatic and narrow-band light sources in the UV region. Nevertheless, more wavelength-specific Φ_λ of actinometers and other reference chemicals are needed that correspond to these newly available light sources, thereby increasing the potential options for using actinometry in varying experimental systems.

Ferrioxalate and iodide-iodate are two standard actinometers that have quantum yields reported at multiple wavelengths.(21-23) Both are used at concentrations that make them optically opaque at wavelengths below 400 nm and 290 nm, respectively. However, these fast-reacting actinometers are not always suitable for use in commercially available benchtop photoreactors that produce high UV light intensities.(24) In addition, actinometers with greater optical transparency are often preferred due to (1) their optical similarity to the organic chemicals typically of interest in these studies and (2) the ability to use the same analytical method to measure the degradation of both the chemical of interest and actinometer (e.g., liquid chromatography with a diode array detector).

Chemicals that have been used as transparent actinometers to measure irradiance across the UV spectrum include nitrate,(23, 25-27) nitrite,(16, 25, 26) hydrogen peroxide,(23, 28-33) uridine,(23, 34, 35) atrazine,(33, 36-41) and p-nitroanisole (PNA).(7, 42) However, there are known limitations in the application of most of these actinometers. Nitrate and nitrite have complex reactions due to the formation of multiple products, with or without the addition of a radical scavenger, and therefore Φ may be affected by the solution pH, actinometer concentration, and scavenger used.(23) Similarly, a high concentration of a radical scavenger is recommended when using hydrogen peroxide as an actinometer to produce a more consistent Φ.(23) For uridine, the reaction kinetic order and Φ were reported to be concentration-dependent and affected by photoproduct absorbance, which are undesired characteristics of an actinometer; nonetheless, an established protocol for uridine actinometry is available in the literature that addresses these constraints.(43) The atrazine Φ has been primarily established at 254 nm within the UVC region,(44, 45) whereas reported Φ for PNA are limited to the UVB and UVA regions.(42) Sulfamethoxazole and diclofenac have also been used as actinometers in recent studies because (1) they can be used with

high UV irradiances that limit the applicability of standard actinometers, and (2) their suitability for field studies due to their presence in natural water bodies.(24, 46) However, a comprehensive characterization of these chemicals for actinometry has not been undertaken.

In addition, previous investigations have shown that different experimental setups, such as the choice of the sample container, can impact observed photolysis rates and consequently impact measured photon irradiances and the apparent Φ.(47-49) While the photochemistry community acknowledges the critical importance of accurate irradiance measurements in determining Φ, the potential errors introduced by varying experimental setups are not typically taken into account. A comprehensive description of experimental setup is commonly not provided, which makes it challenging to discern the cause of discrepancies between reported Φ in the literature.(50-52)

In this study, the impact of experimental setup choices on the apparent Φ were systematically investigated by varying sample containers, the number and position of bulbs, and photoreactor systems. Wavelength-dependent Φ_λ were determined using up to 11 different light sources across the UV spectrum for the popular actinometers uridine, atrazine, and PNA as well as sulfamethoxazole and diclofenac. Lastly, the apparent photon irradiance was calculated using both optically transparent and opaque solutions in a common photoreactor setup (i.e., using test tubes in a merry-go-round) to quantify the potential error introduced based on the choice of the actinometer itself.

EXPERIMENTAL SECTION

Materials. Stock solutions of p-nitroanisole (Acros Organics, 99+% purity), atrazine (Sigma-Aldrich, Pestanal® analytical standard) and sulfamethoxazole (TCI, >98% purity) were prepared in acetonitrile (1 mg/mL, Fisher, HPLC grade), and stock solutions of uridine (Sigma-Aldrich, ≥99% purity) and diclofenac (Sigma-Aldrich, ≥98% purity) were prepared in ultrapure water (7.2 mM and 1 mg/mL, respectively, ≥18.2 MΩ cm, Millipore Direct-Q 3 UV). Working solutions in ultrapure water were prepared at 10 μM for PNA, atrazine, sulfamethoxazole, and diclofenac and 5 μM for uridine. Sulfamethoxazole working solutions were buffered to pH 7.2 or 8 using 0.5 mM phosphate buffer, and uridine working solutions were buffered to pH 7 using 1 mM phosphate buffer. For ferrioxalate actinometry, solutions were prepared at 0.02 M of ferrioxalate in 0.05 M H_2SO_4. More details on solution preparation are in Text S1.

Experimental Setups. Photolysis experiments were performed using either (a) a merry-go-round photoreactor (LZC-4V, Luzchem) with UVC, UVB, or UVA bulbs (irradiance maximum at 254, 313, and 350 nm, respectively), (b) a commercially available LED photoreactor using light centered at 258, 266, or 279 nm (AquiSense PearlLab Beam), (c) a custom-built LED photoreactor(16) using light centered at 276, 316, 346, or 368 nm, or (d) a solar simulator (Oriel Sol1A Class ABB, Newport) (schematics of setups and relative irradiance spectra in Figure 1). The merry-go-round photoreactor featured a ventilation system, internal reflective surfaces, an air temperature display, and a carousel for test tubes made entirely of aluminum. Photographs of all systems and irradiance spectra in photon irradiance units are available in Figure S1. Chemical solutions were added to either a pyrex glass petri dish (50 mm internal diameter, 18 mm depth, 10 mL of solution, 8 mm solution depth) that was transparent or opaque (i.e., painted black, referred to in the text as 'black'), quartz test tubes (10 mm internal diameter, 10 mL of solution), or pyrex

test tubes (10 mm internal diameter, 8 mL of solution). Experiments were conducted independently in at least triplicate and up to seven subsamples of 180 μL were taken during each experiment.

Spectral photon irradiances were obtained from spectroradiometry and/or actinometry. The first approach used direct measurements of the light sources with a spectroradiometer recently calibrated with traceable NIST standards (Black Comet, StellarNet, see Text S3 for setup and testing of the spectroradiometer). Measurements were performed before and after the experiments to verify the light stability throughout the experiments. The spectral irradiances (i.e., in power units of W m^{-2} nm^{-1}) obtained from the spectroradiometer readings were converted to spectral photon irradiances (i.e., in mE cm^{-2} min^{-1} nm^{-1}) for Φ calculations (Text S4). The second approach quantified the spectral photon irradiance using the standard actinometer ferrioxalate with the assumption that the previously published wavelength-dependent Φ_λ were accurate (Text S5).(21) For experiments in petri dishes, the irradiance was corrected by petri factors determined following a published protocol (Text S2, Table S1).(53)

Total photon irradiances summed over the 200-500 nm range varied between 0.2-7% comparing spectroradiometry and ferrioxalate actinometry when using black petri dishes and UVC, UVB, or UVA light sources (merry-go-round photoreactor, 6 bulbs placed at the ceiling, photon irradiance spectrum shown in Figure S4). At the wavelength of the maximum irradiance for these bulbs, the measured irradiance varied by 4-6%. These differences represent an intrinsic uncertainty present when determining Φ_λ due to limitations in accurately quantifying photon irradiance with different approaches.

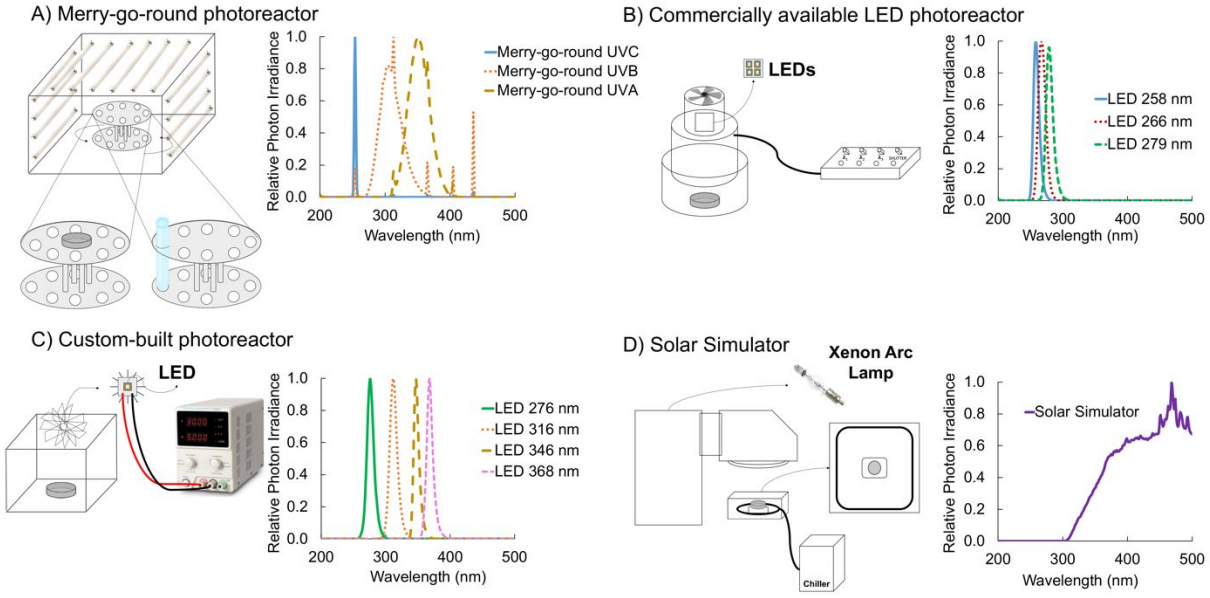

Figure 1. Schematic of setups used in the experiments performed in the (A) merry-go-round photoreactor with a transparent pyrex petri dish, black petri dish, or test tubes, (B) commercially available LED photoreactor, (C) custom-built LED photoreactor, and (D) solar simulator. The relative photon irradiance of light sources available for each of the photoreactors are also shown with the peak wavelength listed in the legend for LED light sources.

Analytical Methods and Photolysis Rates. Chemical degradation was measured by collecting sub-samples at set time intervals during experiments. Analysis of sub-samples used either high-performance liquid chromatography with a diode array detector (HPLC-DAD, Agilent 1260) for atrazine, PNA, sulfamethoxazole, and diclofenac or a UV-vis spectrophotometer (Cary 60, Agilent) using a 1 cm cuvette for ferrioxalate. For uridine, degradation was monitored over time using both HPLC-DAD and UV-vis spectrophotometry at 262 nm with a 1 cm cuvette, the latter following the published protocol for uridine actinometry, to enable a comparison between the two methods.(43) The data obtained from the UV-vis spectrophotometer was observed to deviate

slightly from the data obtained from the HPLC at later time points (i.e, when the uridine concentration decay was above 40%, Figure S6). The slower degradation kinetics observed when using the UV-vis method were attributed to the low absorbance readings between 0.010 and 0.065 in a 1 cm cuvette, which are approaching the instrument's detection limit, and potential interference from the photoproduct absorbance. Therefore, due to the better sensitivity and chromatographic separation possible with the HPLC-DAD, the uridine Φ presented herein were calculated using this method. Method details and information on how pseudo-first-order rate constants were calculated from the observed degradation for all chemicals are provided in Texts S6-S7. For each replicate experiment, linear regression was used to quantify the degradation measured by HPLC-DAD or UV-vis over time until >1-log decay was observed. In experiments requiring >2 hours to reach 1-log decay in the merry-go-round photoreactor, evaporation from the petri dish was observed to be significant even though the maximum air and solution temperatures measured were ≤27 °C. In these cases, experimental times were limited and solution mass was monitored to keep evaporation ≤9.5% of the initial solution mass and maintain log-linear kinetics. Evaporation was not observed in the LED photoreactors or solar simulator due to significantly lower irradiance intensities, which also limits the potential for significant temperature increases, and/or use of a water bath (solar simulator only).

Molar Absorptivity. Molar absorptivities (ε_λ) of transparent chemicals were determined from absorbance data collected using the UV-vis spectrophotometer. A minimum of three solutions with varying concentrations (1-20 mg/L) were prepared in ultrapure water or the previously indicated buffer for the measurements. Quartz cuvettes of 1 and 10 cm pathlengths were used. All measurements were combined and fitted with a series of Gaussian curves to determine the best-fit

values (Text S8, Table S2, Figure S7-S8). Measured molar absorptivities for uridine, atrazine, PNA, and diclofenac were similar to previously reported values.(5, 23, 36, 42, 54) For sulfamethoxazole, the molar absorptivity spectra differed at pH 7.2 and 8 due to the protonation state of the chemical (pK_a=5.9±0.2) and differed from previous findings.(6)

Quantum Yields. Φ_λ of each optically transparent chemical were calculated using Equations 1-2, where k is the pseudo-first-order rate constant for the degradation of that compound, I_λ is the spectral photon irradiance measured by the spectroradiometer, S_λ is the screening factor of the experimental solution, C is the molar concentration of the compound in solution, and l is the solution pathlength. Screening factors are shown in Figure S9.

$$\Phi_\lambda = \frac{k}{2.303 \times \sum_\lambda \varepsilon_\lambda I_\lambda S_\lambda} \qquad (1)$$

$$S_\lambda = \frac{1 - 10^{-\varepsilon_\lambda C\, l}}{2.303\, \varepsilon_\lambda C\, l} \qquad (2)$$

Statistical Analysis. Analysis of significant differences between the experimental data were performed with t-test, with a significance level of $p<0.05$. Relative percent differences between Φ_λ were calculated as either (1) the ratio of the difference between the maximum and minimum Φ and the average Φ to describe variations, (2) the ratio of the difference between the maximum and minimum Φ and the minimum Φ to describe increases, or (3) the ratio of the difference between the maximum and minimum Φ and the maximum Φ to describe decreases. Linear regression statistics and ANOVA tests combined with Dunnett's T3 multiple comparisons statistics were performed to evaluate if Φ_λ calculated at different wavelength ranges were significantly different from each other.

RESULTS AND DISCUSSION

Determining the Optimal Experimental Setup for Calculating Quantum Yields Using a Spectroradiometer. Previous findings have shown that choices in the experimental setup can introduce errors when determining Φ. For instance, direct photolysis rates were observed to be 1.5 to 3 times faster in test tubes compared to open dishes.(47-49) These variations were typically attributed to light reflection in the experimental system and the geometry of the sample container; however, an uneven light field can also introduce experimental error.(55) These errors are often reflected in the variability of reported Φ in the literature. For example, Φ_{254} values for the chemical actinometers atrazine and uridine varied by 33% and 34%, respectively.(23, 43-45, 51, 52, 56-59) Discrepancies in literature values have also prompted studies to revise Φ values for already established actinometers.(42, 60)

Based on previous studies, a petri dish sample container was chosen to determine Φ when using a spectroradiometer to quantify the photon irradiance. This is because the spectroradiometer and the open water surface in the petri dish can both be placed in the same location respective to the downwelling light in each of the photoreactor setups, thereby resulting in the most accurate measurements of fluence. Nevertheless, depending on other experimental setup choices (e.g., using a photoreactor featuring reflective surfaces), the apparent Φ_{UVB} of PNA in a petri dish in the merry-go-round photoreactor varied by up to a factor of 2 (Table 1).

Light Field Uniformity. The light field was characterized with two, four, and six bulbs placed on the ceiling of the merry-go-round (Figure 1A). A more even distribution of light was observed with the maximum of six bulbs installed. Yet, spectroradiometer-measured irradiances still varied

up to 43% between the corners and the center of the photoreactor (Table S3). Over the 5 cm diameter of the petri dish, placed in the center of the photoreactor during experiments, the light field was found to be uniform. Calculated petri factors, which represent the variation in irradiance across the sample container compared to the location of the spectroradiometer measurement, were ≥0.94 regardless of the number of bulbs (Text S2, Table S1). Nevertheless, the petri factors were closer to 1.0 and the calculated apparent Φ were more consistent when using more bulbs (Figure S10, Table S4).

Other minor sources of variability were found to come from the placement of the bulbs and the intensity of the bulbs themselves. The total irradiance ($\sum_{\lambda} I_{200-500\,nm}$) was found to increase approximately proportionally with the number of bulbs installed (Tables S6). However, the measured irradiances normalized by the number of bulbs installed varied up to 18% depending on bulb placement. Part of this observed variability was likely due to differences in irradiances emitted by the individual bulbs, which was found to vary by up to 21% (Table S7).

Light Reflection. Using the black petri dish resulted in a PNA Φ_{UVB} of 0.00032±0.00002, which was not statistically different than the value of 0.00029 determined in a previous study (p=0.15; Table 1).(42) In contrast, using the transparent petri dish resulted in a 92% higher PNA apparent Φ_{UVB}. This higher apparent Φ_{UVB} was attributed to greater effective transmitted irradiance due to light reflection within the photoreactor and sample container that the black petri dish blocks or minimizes, and that cannot be captured by the spectroradiometer that measures only downwelling irradiance, which has been previously reported in the literature.(47-49, 61) Light reflection increases the average pathlength of photons and therefore number of photons available for

photolysis for optically transparent chemicals, resulting in an artificially higher apparent Φ.(49, 62)

The predominant source of light reflection was from the reflective surfaces of the photoreactor (Table 1). Placing black paper between the transparent petri dish and the reflective aluminum surface where the petri dish sat eliminated approximately half of the reflection. Covering all reflective surfaces of the photoreactor with black paper also substantially reduced reflection. However, even in this scenario, using the transparent petri dish still resulted in an 18% higher apparent Φ_{UVB} compared to using the black petri dish. This was attributed to light reflection within the transparent petri dish itself. When using the black petri dish, no significant differences in PNA Φ_{UVB} were observed regardless of whether the reflective surfaces of the photoreactor were covered with black paper. Hence, using the black petri dish minimized potential light reflection during experiments, allowing for the most accurate measurement of photon irradiance to be used to calculate Φ_{UVB}.

Table 1. PNA apparent Φ and standard deviations (SD) obtained in different experimental setups using six UVB bulbs placed on the ceiling of the merry-go-round photoreactor. Samples were rotating in all experiments. Total photon irradiances were obtained using a calibrated spectroradiometer by integrating the irradiance spectrum in the 250-400 nm region, and the values are reported as the average of three independent measurements. Bulb configurations in the photoreactor are illustrated in Figure 1A.

Experimental Setup		**PNA Apparent Φ_{UVB} ± SD**	**Average Measured Photon Irradiance (mE cm^{-2} min^{-1})**
Sample container	**Other**		
Transparent petri dish	n.a.	0.00061 ± 0.00005	0.00089
Transparent petri dish	Merry-go-round covered with black paper	0.00044 ± 0.00004	0.00086

Transparent petri dish	All reflective surfaces of photoreactor covered with black paper	0.00038 ± 0.00003	0.00071
Black petri dish	n.a.	0.00032 ± 0.00002	0.00086
Black petri dish	All reflective surfaces of photoreactor covered with black paper	0.00031 ± 0.00001	0.00066

Wavelength-Dependent Φ_λ for Uridine, Atrazine, PNA, Sulfamethoxazole, and Diclofenac. Based on our initial results, experiments to quantify the Φ_λ of optically transparent chemicals across the UV spectrum were designed to maximize accuracy. This included using the black petri dish to minimize light reflection, characterizing and maximizing the light field uniformity, and verifying a stable irradiance for the duration of experiments. Depending on the molar absorptivity of the chemical, up to 11 different light sources were used to quantify Φ_λ. In addition, at the commonly used concentrations of ≤10 μM and optical path lengths ≤1 cm, screening factors were found to be <0.95 for PNA between 285-350 nm, for sulfamethoxazole <280 nm, and for diclofenac between 255-295 nm (Figure S9). This violates the assumption often relied on when using optically transparent chemical actinometers that <5% of photons are absorbed by the solution. If light screening was not accounted for, calculated Φ_λ would be underestimated by 6-9% for PNA, 5-15% for sulfamethoxazole, and 5-8% for diclofenac for the above-mentioned conditions and depending on the light source used. These differences increase approximately linearly with increases in concentration and path length. Consequently, light screening should be corrected for to calculate accurate Φ_λ.

One discrepancy that was noted when reviewing the literature was the previously reported concentration-dependence of the atrazine Φ_{254}.(44) On examination of the data, we found that the observed behavior could be explained by light screening at high atrazine concentrations. When the

Φ_{254} for each atrazine concentration determined in that study was recalculated by correcting for light screening, a consistent Φ_{254} value with an 8% relative standard deviation was obtained (Table S8). This highlights the importance of verifying that the assumption of optical transparency is valid at the solution concentrations and depths chosen for experiments and correcting for light screening when necessary.

Wavelength-dependent Φ_λ were observed for uridine and atrazine but not for diclofenac. PNA Φ_λ were also wavelength-dependent across the UV spectrum; however, in the wavelength range where it is typically used as an actinometer (i.e., UVB and UVA regions), the wavelength-dependence was minor. Sulfamethoxazole Φ_λ were determined at both pH 7.2 and 8 for comparison with previously reported values.(5, 6) At pH 7.2, sulfamethoxazole is a mixture of protonated and deprotonated species (pK_a=5.9±0.2)(6) and was observed to have a strongly wavelength-dependent Φ_λ ($p=0.004$). Deprotonated sulfamethoxazole did have some statistically distinguishable Φ_λ when comparing results from different light sources, but the overall trend did not show statistically significant wavelength-dependence ($p=0.10$; Figure 2, Tables 3 and S9-S11). Because of these observations, it is strongly recommended that sulfamethoxazole solutions are buffered at pH 8, as minor shifts in the solution pH would introduce substantial error.

The wavelength-independent Φ_λ of deprotonated sulfamethoxazole and diclofenac are desirable, especially when using broadband light sources. Further studies exploring the temperature and concentration-dependence of both sulfamethoxazole and diclofenac Φ_λ, coupled with inter-laboratory comparisons, could position them as viable chemical actinometers for UVC and UVB

light sources. This would expand the list of actinometers available and provide more opportunities to align the molar absorbance and reactivity of the chemical of interest with that of the actinometer.

Wavelength-dependent Φ_λ measured in this work were consistently lower than those reported in the literature (Figure 2).(5, 6, 23, 43-45, 50-52, 56-59, 63) The only exceptions were the PNA Φ_λ in parts of the UVB/UVA region and using the broadband solar simulator, which were similar to the value of 0.00029 previously reported.(42) The lower Φ_λ reported in this work are consistent with our efforts to minimize light reflection to obtain the most accurate measure of irradiance possible, thereby avoiding calculating an artificially higher apparent Φ_λ. Although most of the referenced studies report using transparent dishes or test tubes as sample containers, detailed descriptions of photoreactor setups were usually absent. This makes it challenging to discern the cause of the discrepancies in reported Φ_λ.

To evaluate whether Φ_λ were reproducible across photoreactors when care was taken to optimize the experimental setup, four pairs of light sources with similar spectra were compared (Figure 3). There was good agreement between light source pairs with differences in measured Φ_λ being ≤20% (Table S12). However, the observed differences of 13% for deprotonated sulfamethoxazole ($p=0.0008$) and 20% for atrazine ($p<0.0001$) under UVC light exposure (λ=252-264 nm) were statistically different and are believed to reflect actual differences in Φ_λ over a narrow wavelength range and not be caused by experimental artifacts. This was supported by the consistency of the data, exhibiting relative standard deviations ≤7% across multiple experiments with independent measurements of irradiance (n=4-8). If the differences were due to a systematic bias between

photoreactors, these differences should have been observed across all chemicals and not only atrazine and deprotonated sulfamethoxazole.

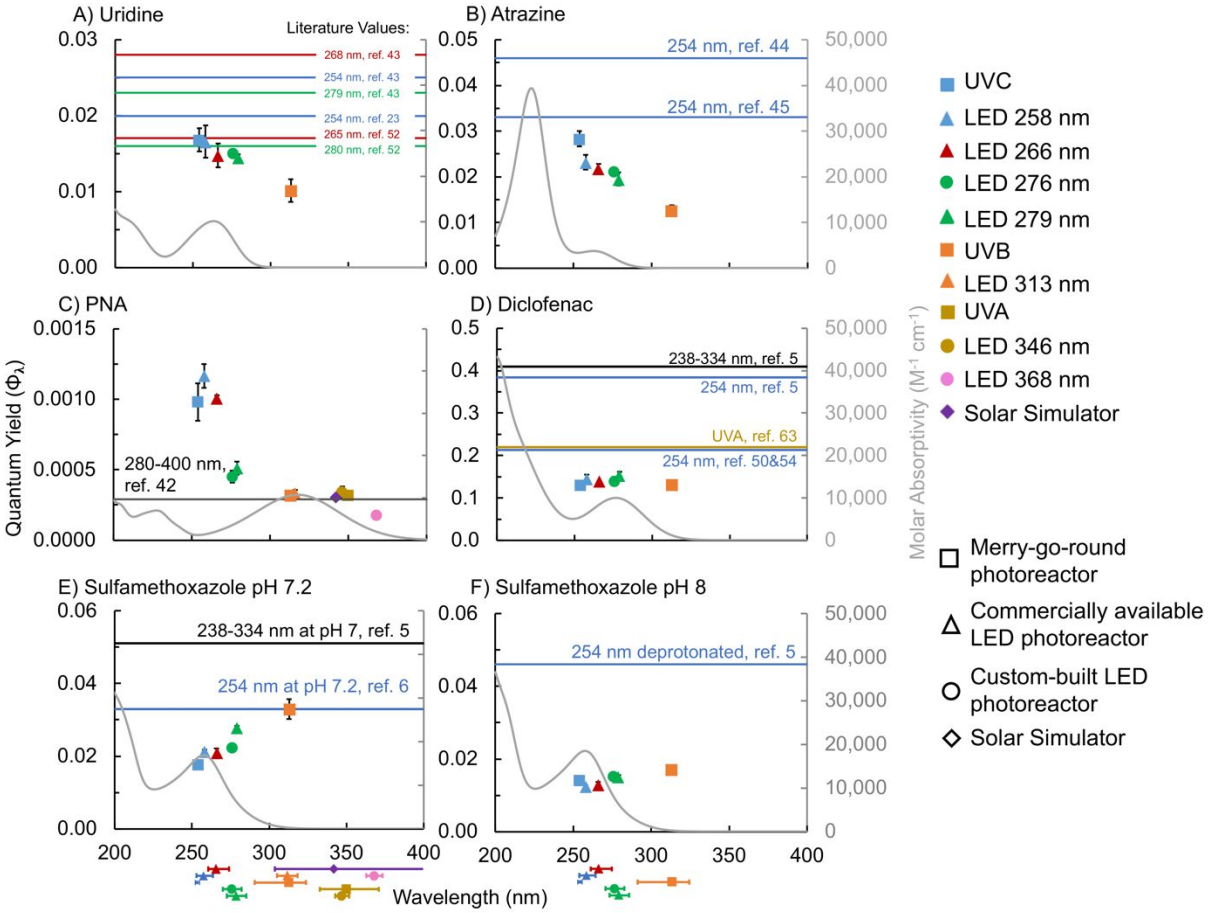

Figure 2. Quantum yields (left axis) for (A) uridine, (B) atrazine, (C) PNA, (D) diclofenac, (E) sulfamethoxazole pH 7.2, and (F) sulfamethoxazole pH 8 determined using multiple light sources with symbols representing the photoreactor type and colors representing the irradiance region (also see Tables 3 and S8 for Φ_λ values). Molar absorptivities for each actinometer are shown as solid gray lines (right axis). Colored horizontal bars at the bottom of the figure represent the wavelength range of the light sources with symbols indicating the wavelength of the maximum irradiance and the bar representing the full width at half maximum. Φ_λ values reported in the literature are

included as solid horizontal lines. Chemical degradation over time plots for all experiments are available in Figure S13.

Table 3. Measured average Φ_λ, their standard deviation, and the number of replicate experiments conducted (n) for uridine, atrazine, PNA, diclofenac, and deprotonated sulfamethoxazole determined using multiple light sources and the black petri dish. For deprotonated sulfamethoxazole and diclofenac, for which there appeared to be no wavelength dependence, average Φ_λ were calculated using all results. Values for sulfamethoxazole at pH 7.2 are available in Table S8. Regression and ANOVA statistical test results comparing the Φ_λ obtained with different light sources can be found in Tables S9-S10. Chemical degradation over time plots for all experiments are available in Figure S13.

Light Region	Experimental Setup	*n*	Quantum Yield (Φ_λ) ± SD
Uridine			
UVC	Merry-go-round UVC (max. 254 nm)	11	0.0168 ± 0.0015
	Commercially-available LED 258 nm	6	0.0165 ± 0.0021
	Commercially-available LED 266 nm	3	0.0148 ± 0.0016
UVC/UVB	Custom-built LED 276 nm	3	0.0150 ± 0.0003
	Commercially-available LED 279 nm	3	0.0145 ± 0.0005
	UVB (max. 313 nm)	3	0.0101 ± 0.0015
Atrazine			
UVC	Merry-go-round UVC (max. 254 nm)	8	0.0283 ± 0.0017
	Commercially-available LED 258 nm	6	0.0232 ± 0.0016
	Commercially-available LED 266 nm	3	0.0218 ± 0.0010
UVC/UVB	Custom-built LED 276 nm	4	0.0212 ± 0.0008
	Commercially-available LED 279 nm	4	0.0195 ± 0.0014
	Merry-go-round UVB (max. 313 nm)	3	0.0126 ± 0.0011
PNA			
UVC	Merry-go-round UVC (max. 254 nm)	3	0.00098 ± 0.00013
	Commercially-available LED 258 nm	3	0.00116 ± 0.00009
	Commercially-available LED 266 nm	3	0.00101 ± 0.00002
UVC/UVB	Custom-built LED 276 nm	3	0.00045 ± 0.00004
	Commercially-available LED 279 nm	3	0.00051 ± 0.00005
	Merry-go-round UVB (max. 313 nm)	3	0.00032 ± 0.00002
	Custom-built LED 316 nm	3	0.00033 ± 0.00002

UVA	Merry-go-round UVA (max. 350 nm)	3	0.00031 ± 0.00002
	Custom-built LED 346 nm	3	0.00034 ± 0.00004
	Custom-built LED 368 nm	3	0.00017 ± 0.00001
UV-visible	Solar Simulator	3	0.00031 ± 0.00002
Diclofenac			
UVC	Merry-go-round UVC (max. 254 nm)	3	0.129 ± 0.009
	Commercially-available LED 258 nm	3	0.144 ± 0.012
	Commercially-available LED 266 nm	3	0.138 ± 0.002
UVC/UVB	Custom-built LED 276 nm	3	0.139 ± 0.005
	Commercially-available LED 279 nm	3	0.152 ± 0.010
	Merry-go-round UVB (max. 313 nm)	3	0.130 ± 0.010
	Average ± St. Dev.		0.139 ± 0.009
Sulfamethoxazole pH 8			
UVC	Merry-go-round UVC (max. 254 nm)	6	0.0164 ± 0.0004
	Commercially-available LED 258 nm	4	0.0144 ± 0.0005
	Commercially-available LED 266 nm	3	0.0145 ± 0.0011
UVC/UVB	Custom-built LED 276 nm	3	0.0164 ± 0.0011
	Commercially-available LED 279 nm	3	0.0160 ± 0.0006
	Merry-go-round UVB (max. 313 nm)	3	0.0178 ± 0.0006
	Average ± St. Dev.		0.0159 ± 0.0013

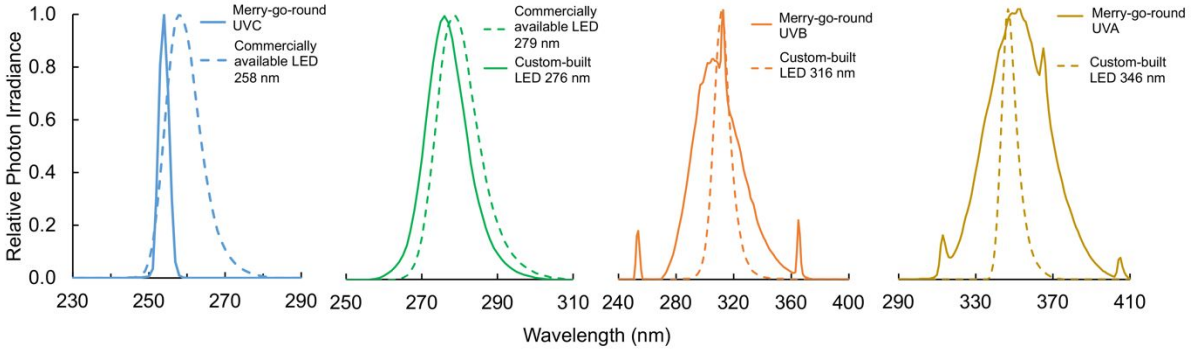

Figure 3. Relative photon irradiances of the light sources used to evaluate the reproducibility of Φ_λ measured across photoreactors.

Measuring the Photon Irradiances Received by Transparent and Opaque Solutions. Photoreactors equipped with a merry-go-round configuration with bulbs positioned on multiple sides are commonly used in photochemical studies.(7, 64-76) This experimental setup allows for

multiple samples to be irradiated simultaneously and promotes light field uniformity by rotating the samples. However, measuring representative photon irradiance using a spectroradiometer in this setup is not possible. While actinometers are preferred in such scenarios, a direct comparison of multiple actinometers to quantify photon irradiances within this configuration could not be found in the literature.

To compare the performance of transparent and opaque solutions in quantifying photon irradiances, experiments were conducted using test tubes that were rotating in the reflective merry-go-round photoreactor. Solutions were irradiated simultaneously with either eight UVC or UVB bulbs placed on the sides of the photoreactor (setup in Figure 1A). Total photon irradiance was calculated from the photodegradation rates of each chemical using the Φ_λ from Table 3 and published values for ferrioxalate (Equations 1-2 and S2).(21) Results showed that photon irradiances measured by optically transparent solutions were 1.6 to 4.5 times greater than those measured by ferrioxalate (Figure 4, Table S13).

Lower irradiances were measured with ferrioxalate because it absorbs all light <400 nm, whereas light can reflect off the inner walls of the photoreactor and test tubes and remain available for photolysis when irradiating transparent solutions. These findings are consistent with the observations described in the previous sections and those reported by previous studies.(47-49, 77) Ferrioxalate has been used as an actinometer to determine photon irradiances in merry-go-round photoreactors by several studies.(67-76) However, these findings show that transparent chemical actinometers, and not ferrioxalate, should be used when the experimental solutions are themselves transparent. Ferrioxalate could still be used if reflection in the experimental setup is eliminated

(e.g., using a black petri dish) or if the experimental solution being evaluated is optically opaque. For example, in the previous study that reported atrazine Φ_{254} at varying concentrations, the Φ_{254} reported at high concentrations converged with the value found in this work;(44) this is because the solution was becoming optically opaque at high concentrations and ferrioxalate was used as the actinometer.

When comparing transparent solutions only, measured irradiances were in good agreement when using UVC bulbs with differences ≤23% (Figure 4A). Results from experiments using UVB bulbs, however, showed substantially higher irradiances measured by uridine and atrazine than the other transparent chemicals even though the Φ_{UVB} determined in the petri dish setup were used (Figure 4B). Notably, the UVB bulbs include a spectral band in the UVC centered at 254 nm, and both uridine and atrazine have higher Φ and similar ε in the UVC compared to the UVB region (Figure 2 and S17). While PNA also has a higher Φ in the UVC, its ε is substantially lower in the UVC region compared to the UVB region. Therefore, it was hypothesized that the presence of UVC light was disproportionately affecting the irradiances measured by uridine and atrazine.

To minimize the transmittance of UVC light emitted by the UVB bulbs, solutions of all chemicals were irradiated in pyrex test tubes instead of quartz test tubes (i.e., pyrex screens light <315 nm), which resulted in total irradiance measured by the transparent solutions being ≤23% (Figure 4C, Figure S16). Therefore, the erroneously higher irradiances observed for uridine and atrazine in quartz tubes were attributed to differing degrees of reflection of UVC and UVB light. This is also supported by the observed ratio of irradiances between transparent solutions and ferrioxalate in Figures 4A and 4B. Similarly, the differences observed between the transparent solutions were

also attributed to the wavelength-dependent nature of light reflection coupled with the differing molar absorptivities of the chemicals. These results highlight the benefits of choosing an actinometer with similar photochemical properties to the chemical of interest to account for the occurrence of light reflection. However, there will always be some differences between the actinometer and chemical of interest and the variations quantified here (up to 23% relative differences) can be considered as a degree of intrinsic uncertainty present when using actinometry to calculate unknown quantum yields.

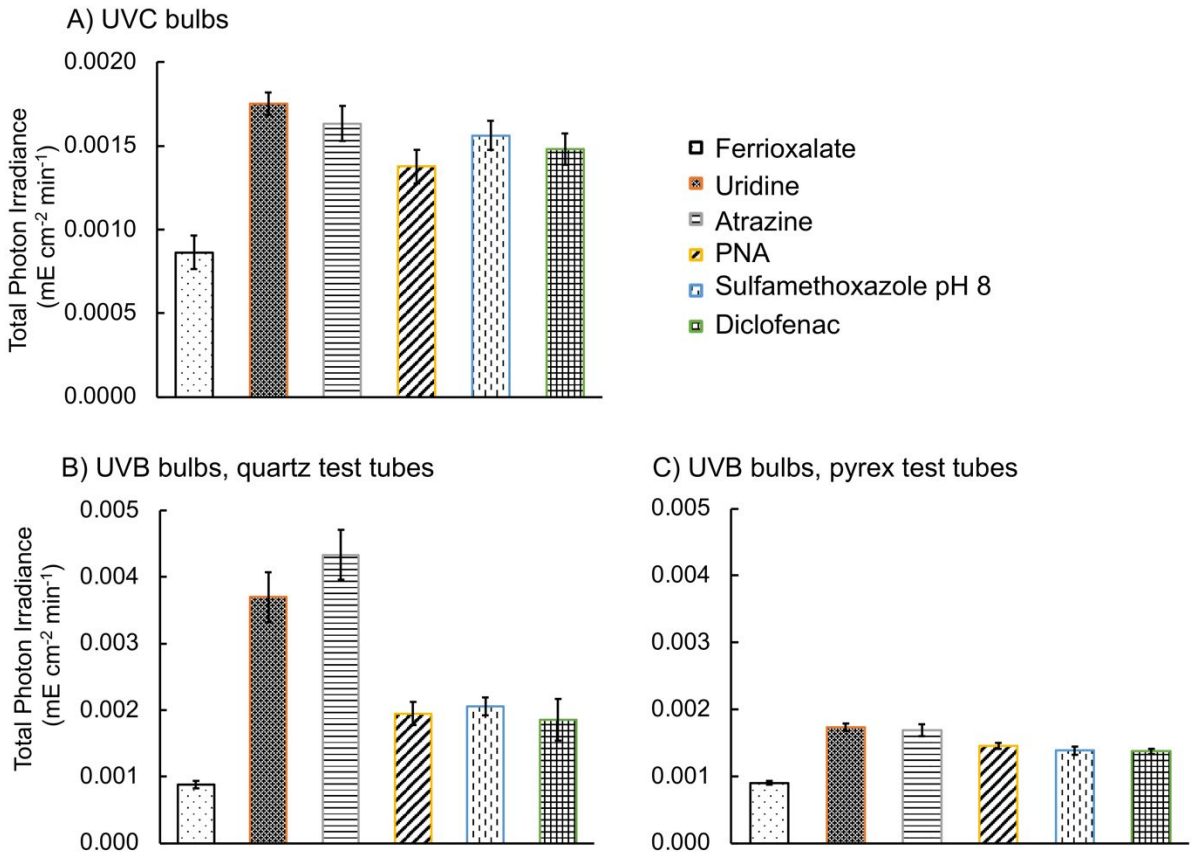

Figure 4. Total photon irradiances ($\sum I_{200-500\,nm}$) and standard errors measured by each chemical during experiments using either eight (A) UVC bulbs or (B and C) UVB bulbs in the merry-go-round photoreactor. Experiments with UVB bulbs were performed either with (B) quartz test tubes or (C) pyrex test tubes that were rotating. Irradiances were calculated using Equations 1-2 for

uridine, atrazine, PNA, sulfamethoxazole, and diclofenac, and using Equation S2 for ferrioxalate. Statistical comparisons are presented in Table S13. All chemicals were simultaneously irradiated to mitigate the effects of light fluctuations. Time points were selected to allow for at least one complete rotation of the tubes in the merry-go-round and based on their respective photodegradation rates. The Φ_λ measured in this work (Table 3) were used to calculate the total photon irradiances and ferrioxalate Φ_λ values were from the literature.(21) Chemical degradation over time plots for each of the experiments are available in Figure S15.

IMPLICATIONS

As shown in this work, an optimized experimental setup is critical when using a spectroradiometer to measure incident photon irradiances. In comparison, the use of actinometers allows for more flexibility including more choices in photoreactor and sample container geometries and the ability to capture the effects of light reflection and varying bulb intensities. Importantly, actinometry allows for irradiating multiple experimental solutions simultaneously in the merry-go-round photoreactor. Nevertheless, care should be taken in selecting an appropriate actinometer as differences in molar absorptivity spectra and photoreactivity resulted in variations in measured irradiance, especially when using a broadband light source or actinometer with a wavelength-dependent Φ_λ. However, the variations observed were relatively minor (differences of ≤23%), and spectroradiometry is also susceptible to measurement errors due to the need for ongoing calibration and the limitations of the sensor and its placement. Consequently, actinometry is usually preferable and the addition of Φ_λ for more chemicals to the literature will increase our ability to measure and model the photochemical fate of chemicals of interest.

This work characterizes the wavelength-dependence of Φ_λ of several commonly used actinometers using up to 11 different light sources. In addition, Φ_λ were determined for sulfamethoxazole and diclofenac, which have been previously used to quantify irradiance. Although sulfamethoxazole and diclofenac are not currently considered actinometers, their wavelength-independent Φ is a desirable attribute and makes them potentially viable actinometers in the UVC/UVB regions. The Φ_λ of PNA, a commonly used actinometer for the UVB and UVA regions, was also characterized for UVC light sources. The addition of PNA provides an actinometer with substantially slower kinetics making it a better candidate to investigate chemicals with lower photoreactivity. In turn, these reported values can be referenced to investigate the wavelength-dependence of photodegradation for other chemicals of interest using actinometry.

ACKNOWLEDGEMENTS

This research was supported by the United States Department of Agriculture (USDA NIFA grant number 2022-67020-37182). The authors would like to thank Casey Bloomquist for building the LED photoreactor.

CONFLICTS OF INTEREST

There are no conflicts to declare.

REFERENCES

1. Ossola R, Clerc B, McNeill K. Mechanistic Insights into Dissolved Organic Sulfur Photomineralization through the Study of Cysteine Sulfinic Acid. Environ Sci Technol. 2020;54(20):13066-76.

2. McNeill K, Canonica S. Triplet state dissolved organic matter in aquatic photochemistry: reaction mechanisms, substrate scope, and photophysical properties. Environ Sci Process Impacts. 2016;18(11):1381-99.

3. Apell JN, Kliegman S, Sola-Gutierrez C, McNeill K. Linking Triclosan's Structural Features to Its Environmental Fate and Photoproducts. Environ Sci Technol. 2020;54(22):14432-41.

4. Silverman AI, Sedlak DL, Nelson KL. Simplified Process to Determine Rate Constants for Sunlight-Mediated Removal of Trace Organic and Microbial Contaminants in Unit Process Open-Water Treatment Wetlands. Environmental Engineering Science. 2019;36(1):43-59.

5. Canonica S, Meunier L, von Gunten U. Phototransformation of selected pharmaceuticals during UV treatment of drinking water. Water Res. 2008;42(1-2):121-8.

6. Carlson JC, Stefan MI, Parnis JM, Metcalfe CD. Direct UV photolysis of selected pharmaceuticals, personal care products and endocrine disruptors in aqueous solution. Water Res. 2015;84:350-61.

7. Apell JN, Pflug NC, McNeill K. Photodegradation of Fludioxonil and Other Pyrroles: The Importance of Indirect Photodegradation for Understanding Environmental Fate and Photoproduct Formation. Environ Sci Technol. 2019;53(19):11240-50.

8. Lu Z, Challis JK, Wong CS. Quantum Yields for Direct Photolysis of Neonicotinoid Insecticides in Water: Implications for Exposure to Nontarget Aquatic Organisms. Environmental Science & Technology Letters. 2015;2(7):188-92.

9. Wu B, Arnold WA, Ma L. Photolysis of atrazine: Role of triplet dissolved organic matter and limitations of sensitizers and quenchers. Water Res. 2021;190:116659.

10. Hora PI, Arnold WA. Photochemical fate of quaternary ammonium compounds in river water. Environ Sci Process Impacts. 2020;22(6):1368-81.

11. Ossola R, Jonsson OM, Moor K, McNeill K. Singlet Oxygen Quantum Yields in Environmental Waters. Chem Rev. 2021;121(7):4100-46.

12. Canonica S, Jans U, Stemmler K, Hoigne J. Transformation Kinetics of Phenols in Water: Photosensitization by Dissolved Natural Organic Material and Aromatic Ketones. Environ Sci Technol. 1995;29:1822-31.

13. Hora PI, Novak PJ, Arnold WA. Photodegradation of pharmaceutical compounds in partially nitritated wastewater during UV irradiation. Environmental Science: Water Research & Technology. 2019;5(5):897-909.

14. Remke SC, von Gunten U, Canonica S. Enhanced transformation of aquatic organic compounds by long-lived photooxidants (LLPO) produced from dissolved organic matter. Water Res. 2021;190:116707.

15. Partanen SB, Erickson PR, Latch DE, Moor KJ, McNeill K. Dissolved Organic Matter Singlet Oxygen Quantum Yields: Evaluation Using Time-Resolved Singlet Oxygen Phosphorescence. Environ Sci Technol. 2020;54(6):3316-24.

16. Ward CP, Bowen JC, Freeman DH, Sharpless CM. Rapid and Reproducible Characterization of the Wavelength Dependence of Aquatic Photochemical Reactions Using Light-Emitting Diodes. Environmental Science & Technology Letters. 2021;8(5):437-42.

17. Wan D, Yang J, Wang X, Xiang W, Selvinsimpson S, Chen Y. Wavelength-Dependent Photoreactivity of Root Exudates from Aquatic Plants under UV-LED Irradiation. ACS ES&T Water. 2022;2(12):2613-22.

18. Wang Y, Wu B, Zheng X, Chen B, Chu C. Assessing the quantum yield spectrum of photochemically produced reactive intermediates from black carbon of various sources and properties. Water Res. 2023;229:119450.

19. Bhat AP, Pomerantz WCK, Arnold WA. Wavelength-Dependent UV-LED Photolysis of Fluorinated Pesticides and Pharmaceuticals. Environ Sci Technol. 2023;57(13):5327-36.

20. Zhou C, Wu B, Zheng X, Chen B, Chu C. Wavelength-dependent direct and indirect photochemical transformations of organic pollutants. Sci Total Environ. 2024;916:170414.

21. Goldstein S, Rabani J. The ferrioxalate and iodide–iodate actinometers in the UV region. Journal of Photochemistry and Photobiology A: Chemistry. 2008;193(1):50-5.

22. Bolton JR, Stefan MI, Shaw P-S, Lykke KR. Determination of the quantum yields of the potassium ferrioxalate and potassium iodide–iodate actinometers and a method for the calibration of radiometer detectors. Journal of Photochemistry and Photobiology A: Chemistry. 2011;222(1):166-9.

23. Rabani J, Mamane H, Pousty D, Bolton JR. Practical Chemical Actinometry-A Review. Photochemistry and Photobiology. 2021;97(5):873-902.

24. Bulman DM, Mezyk SP, Remucal CK. The Impact of pH and Irradiation Wavelength on the Production of Reactive Oxidants during Chlorine Photolysis. Environ Sci Technol. 2019;53(8):4450-9.

25. Jankowski JJ, Kieber DJ, Mopper K. Nitrate and Nitrite Ultraviolet Actinometers. Photochemistry and Photobiology. 2008;70(3):319-28.

26. Xue L, Kieber DJ. Photochemical Production and Photolysis of Acrylate in Seawater. Environ Sci Technol. 2021;55(10):7135-44.

27. DiMento BP, Tusei CL, Aeppli C. Photochemical degradation of short-chain chlorinated paraffins in aqueous solution by hydrated electrons and hydroxyl radicals. Chemosphere. 2022;303(Pt 1):134732.

28. Mazellier P, Meite L, De Laat J. Photodegradation of the steroid hormones 17beta-estradiol (E2) and 17alpha-ethinylestradiol (EE2) in dilute aqueous solution. Chemosphere. 2008;73(8):1216-23.

29. Benitez FJ, Acero JL, Real FJ, Roldan G, Rodriguez E. Photolysis of model emerging contaminants in ultra-pure water: kinetics, by-products formation and degradation pathways. Water Res. 2013;47(2):870-80.

30. Wang L, Chen Y, Chen B, Yang J. Generation of hydroxyl radicals during photodegradation of chloroacetic acids by 254 nm ultraviolet: A special degradation process revealed by a holistic radical determination methodology. J Hazard Mater. 2021;404(Pt B):124040.

31. Djebbar KE, Zertal A, Debbache N, Sehili T. Comparison of Diuron degradation by direct UV photolysis and advanced oxidation processes. J Environ Manage. 2008;88(4):1505-12.

32. Hykrdova L, Bajt O, Jirkovsky J. Mechanism and kinetics of photochemical transformation of ketoprofen and its degradation intermediates. J Hazard Mater. 2018;353:70-9.

33. Jia L, Chen R, Sun Z, Li W, Wang H, Qiang Z. Degradation of micropollutants in flow-through VUV/UV reactors: Impact of internal diameter and baffle allocation. Chemosphere. 2023;335:139112.

34. Gurzadyan GG, Gorner H. Depopulation of highly excited singlet states of DNA model compounds: quantum yields of 193 and 245 nm photoproducts of pyrimidine monomers and dinucleoside monophosphates. Photochemistry and Photobiology. 1996;63(2):143-53.

35. Marks RGH, Drees F, Rockel S, Kerpen K, Jochmann MA, Schmidt TC. Mechanistic investigation of phosphonate photolysis in aqueous solution by simultaneous LC-IRMS and HRMS analysis. Journal of Photochemistry and Photobiology A: Chemistry. 2023;439.

36. Salgado R, Pereira VJ, Carvalho G, Soeiro R, Gaffney V, Almeida C, et al. Photodegradation kinetics and transformation products of ketoprofen, diclofenac and atenolol in pure water and treated wastewater. J Hazard Mater. 2013;244-245:516-27.

37. Xiao Y, Fan R, Zhang L, Yue J, Webster RD, Lim TT. Photodegradation of iodinated trihalomethanes in aqueous solution by UV 254 irradiation. Water Res. 2014;49:275-85.

38. Liu WR, Ying GG, Zhao JL, Liu YS, Hu LX, Yao L, et al. Photodegradation of the azole fungicide climbazole by ultraviolet irradiation under different conditions: Kinetics, mechanism and toxicity evaluation. J Hazard Mater. 2016;318:794-801.

39. Prados-Joya G, Sanchez-Polo M, Rivera-Utrilla J, Ferro-Garcia M. Photodegradation of the antibiotics nitroimidazoles in aqueous solution by ultraviolet radiation. Water Res. 2011;45(1):393-403.

40. Yuan F, Hu C, Hu X, Qu J, Yang M. Degradation of selected pharmaceuticals in aqueous solution with UV and UV/H(2)O(2). Water Res. 2009;43(6):1766-74.

41. Hermosillo-Arellano E, Ocampo-Perez R, Sanchez-Polo AM, Sanchez-Polo M, Flores-Vélez LM, Mendoza-Mendoza E. Role of the radical promoter systems on the degradation of an antipeleptic drug using HO and SO4- species. Journal of Water Process Engineering. 2019;27:162-70.

42. Laszakovits JR, Berg SM, Anderson BG, O'Brien JE, Wammer KH, Sharpless CM. p-Nitroanisole/Pyridine and p-Nitroacetophenone/Pyridine Actinometers Revisited: Quantum Yield in Comparison to Ferrioxalate. Environmental Science & Technology Letters. 2017;4(1):11-4.

43. Pousty D, Mamane H, Cohen-Yaniv V, Bolton JR. Protocol for UVC uridine actinometry. MethodsX. 2023;10:101957.

44. Hessler DP, Gorenflo V, Frimmel FH. Degradation of Aqueous Atrazine and Metazachlor Solutions by UV and UV/H2O2 — Influence of pH and Herbicide Concentration Abbau von Atrazin und Metazachlor in wäßriger Lösung durch UV und UV/H2O2 — Einfluß von pH und Herbizid-Konzentration. Acta hydrochimica et hydrobiologica. 2006;21(4):209-14.

45. Bolton JR, Stefan MI. Fundamental photochemical approach to the concepts of fuence (UV dose) and electrical energy efficiency in photochemical degradation reactions. Res Chem Intermed. 2022;28:857-70.

46. Schmitt M, Wack K, Glaser C, Wei R, Zwiener C. Separation of Photochemical and Non-Photochemical Diurnal In-Stream Attenuation of Micropollutants. Environ Sci Technol. 2021;55(13):8908-17.

47. Dulln D, Mill T. Development and Evaluation of Sunlight Actinometers. Environ Sci Technol. 1982;16:815-20.

48. Haag WR, Hoigne J. Singlet Oxygen in Surface Waters: Photochemical Formation and Steady-State Concentrations in Various Types of Waters. Environ Sci Technol. 1986;20:341-8.

49. Zepp RG, Cline DM. Rates of Direct Photolysis in Aquatic Environment. Environ Sci Technol. 1977;11(4):359-66.

50. Baeza C, Knappe DR. Transformation kinetics of biochemically active compounds in low-pressure UV photolysis and UV/H(2)O(2) advanced oxidation processes. Water Res. 2011;45(15):4531-43.

51. Gorner H. Chromophore loss of uracil derivatives and polyuridylic acid in aqueous solution caused by 248 run laser pulses and continuous UV irradiation: mechanism of the photohydration of pyrimidines. Journal of Photochemistry and Photobiology B: Biology. 1991;10:91-110.

52. Kuhn HJ, Braslavsky SE, Schmidt R. Chemical Actinometry. Pure Appl Chem. 1989;61:187-210.

53. Bolton JR, Beck S, Linden KG. Protocol for the determination of fluence (UV dose) using a low-pressure or low-pressure high-output UV lamp in benchscale collimated beam ultraviolet experiments. International Ultraviolet Association. 2003.

54. Ericksson J, Svanfelt J, Kronberg L. A Photochemical Study of Diclofenac and Its Major Transformation Products. Photochemistry and Photobiology. 2010;86:528-32.

55. Bolton JR, Linden KG. Standardization of Methods for Fluence (UV Dose) Determination in Bench-Scale UV Experiments. J Environ Eng. 2003;129:209-15.

56. Linden KG, Darby JL. Estimating Effective Germicidal Dose From Medium Pressure UV Lamps. J Environ Eng 1997;123 (11) 1142-9.

57. Sinsheimer RL. The Photochemistry of Uridylic Acid. Radiation Research. 1954;1:505-13.

58. Swenson PA, Setlow RB. Kinetics of Dimer Formation and Photohydration in Ultraviolet-Irradiated Polyuridylic Acid. Photochemistry and Photobiology. 2008;2(4):419-34.

59. Pousty D, Mamane H, Cohen-Yaniv V, Bolton JR. Ultraviolet actinometry – Determination of the incident photon flux and quantum yields for photochemical systems using low-pressure and ultraviolet light-emitting diode light sources. Journal of Environmental Chemical Engineering. 2022;10(3).

60. Galbavy ES, Ram K, Anastasio C. 2-Nitrobenzaldehyde as a chemical actinometer for solution and ice photochemistry. Journal of Photochemistry and Photobiology A: Chemistry. 2010;209(2-3):186-92.

61. Lin J, Apell JN, McNeill K, Emberger M, Ciraulo V, Gimeno S. A streamlined workflow to study direct photodegradation kinetic and transformation products for persistence assessment of a fragrance ingredient in natural waters. Environ Sci Process Impacts. 2019;21(10):1713-21.

62. Apell JN, McNeill K. Updated and validated solar irradiance reference spectra for estimating environmental photodegradation rates. Environ Sci Process Impacts. 2019;21(3):427-37.

63. Moore DE, Roberts-Thomson S, Zhen D, Duke CC. Photochemical studies on the anti-inflammatory drug diclofenac. Photochem Photobiol. 1990;52(4):685-90.

64. Couch K, Leresche F, Farmer C, McKay G, Rosario-Ortiz FL. Assessing the source of the photochemical formation of hydroxylating species from dissolved organic matter using model sensitizers. Environ Sci Process Impacts. 2022;24(1):102-15.

65. Tsui SM, Chu W. Quantum yield study of the photodegradation of hydrophobic dyes in the presence of acetone sensitizer. Chemosphere. 2001;44(1):17-22.

66. Wang J, Chen J, Qiao X, Wang Y, Cai X, Zhou C, et al. DOM from mariculture ponds exhibits higher reactivity on photodegradation of sulfonamide antibiotics than from offshore seawaters. Water Res. 2018;144:365-72.

67. Parker KM, Pignatello JJ, Mitch WA. Influence of ionic strength on triplet-state natural organic matter loss by energy transfer and electron transfer pathways. Environ Sci Technol. 2013;47(19):10987-94.

68. Chu W, Jafvert CT. Photodechlorination of Polychlorobenzene Congeners in Surfactant Micelle Solutions. Environ Sci Technol. 1994;28:2415-22.

69. Mateus MCDA, Silva AM, Burrows HD. Environmental and laboratory studies of the photodegradation of the pesticide fenarimol. Journal of Photochemistry and Photobiology A: Chemistry. 1994;80:409-16.

70. Chu W. Photodechlorination Mechanism of DDT in a UV/Surfactant System. Environ Sci Technol. 1999;33:421-5.

71. Hou WC, Stuart B, Howes R, Zepp RG. Sunlight-driven reduction of silver ions by natural organic matter: formation and transformation of silver nanoparticles. Environ Sci Technol. 2013;47(14):7713-21.

72. Chu W, Chan KH, Kwan CY, Jafvert CT. Acceleration and Quenching of the Photolysis of PCB in the Presence of Surfactant and Humic Materials. Environ Sci Technol. 2005;39:9211-6.

73. Grebel JE, Pignatello JJ, Mitch WA. Impact of halide ions on natural organic matter-sensitized photolysis of 17beta-estradiol in saline waters. Environ Sci Technol. 2012;46(13):7128-34.

74. Odum JR, McDow SR, Kamens RM. Mechanistic and Kinetic Studies of the Photodegradation of Banz[a]anthracene in the Presence of Methoxyphenols. Environ Sci Technol. 1994;28:1285-90.

75. Adak A, Mangalgiri KP, Lee J, Blaney L. UV irradiation and UV-H(2)O(2) advanced oxidation of the roxarsone and nitarsone organoarsenicals. Water Res. 2015;70:74-85.

76. Martin MA, Sivaguru J, McEvoy J, Sonthiphand P, Delorme A, Khan E. Photodegradation of (E)- and (Z)-Endoxifen in water by ultraviolet light: Efficiency, kinetics, by-products, and toxicity assessment. Water Res. 2020;171:115451.

77. Nicole I, Laat JD, Dore M, Duguet JP, Bonnel C. Use of UV Radiation in Water Treatment: Measurement of Photonic Flux by Hydrogen Peroxide Actinometry. Water Res. 1990;24:157-68.